UC Irvine
UC Irvine Previously Published Works

Title

Closing the Winter Gap—Year-Round Measurements of Soil CO2 Emission Sources in Arctic Tundra

Permalink

Journal

ISSN

Authors

Pedron, Shawn A
Welker, JM
Euskirchen, ES
et al.

Publication Date

DOI

Copyright Information

Peer reviewed

Key Points:
- Combining continuous soil CO_2 flux with $\Delta^{14}CO_2$ observations enables a systematic evaluation of carbon cycling in Arctic soils year-round
- Outside the growing season, soil microorganisms rely on older, local soil carbon pools not captured in short-term incubation experiments
- Permafrost warming and thaw is depleting soil carbon pools; fluxes of older carbon are greatest in summer but dominate emissions in winter

Closing the Winter Gap—Year-Round Measurements of Soil CO_2 Emission Sources in Arctic Tundra

Shawn A. Pedron[1] ⓘ, J. M. Welker[2,3,4] ⓘ, E. S. Euskirchen[5] ⓘ, E. S. Klein[6] ⓘ, J. C. Walker[7], X. Xu[1] ⓘ, and C. I. Czimczik[1] ⓘ

[1]Department of Earth System Science, University of California, Irvine, CA, USA, [2]Department of Biological Sciences, University of Alaska Anchorage, Anchorage, AK, USA, [3]University of Oulu, Oulu, Finland, [4]UArctic, Rovaniemi, Finland, [5]Institute of Arctic Biology, University of Alaska, Fairbanks, AK, USA, [6]Department of Geological Sciences, University of Alaska Anchorage, Anchorage, AK, USA, [7]A. E. Lalonde AMS Laboratory, Ottawa, ON, Canada

Abstract Non-growing season CO_2 emissions from Arctic tundra remain a major uncertainty in forecasting climate change consequences of permafrost thaw. We present the first time series of soil and microbial CO_2 emissions from a graminoid tundra based on year-round in situ measurements of the radiocarbon content of soil CO_2 ($\Delta^{14}CO_2$) and of bulk soil C ($\Delta^{14}C$), microbial activity, and temperature. Combining these data with land-atmosphere CO_2 exchange allows estimates of the proportion and mean age of microbial CO_2 emissions year-round. We observe a seasonal shift in emission sources from fresh carbon during the growing season (August $\Delta^{14}CO_2 = 74 \pm 4.7‰$, 37% $\pm$ 3.4% microbial, mean $\pm$ se) to increasingly older soil carbon in fall and winter (March $\Delta^{14}CO_2 = 22 \pm 1.3‰$, 47% $\pm$ 8% microbial). Thus, rising soil temperatures and emissions during fall and winter are depleting aged soil carbon pools in the active layer and thawing permafrost and further accelerating climate change.

Plain Language Summary The Arctic is warming and large quantities of organic matter in permafrost soils are at risk of becoming decomposed to carbon dioxide (CO_2) by microbes. Measurements of soil CO_2 emissions do not provide direct estimates of permafrost emissions, however, because CO_2 is produced by microbes and plant roots. Using a new sampler, we collected soil CO_2 in northern Alaska over 3–6 weeks for 2 years and analyzed its radiocarbon content to distinguish CO_2 sources. To calculate CO_2 budgets, we added observations of soil and microbial CO_2 emissions and soil temperature. We find that microbes rely on fresh plant matter in summer but older organic matter from fall to spring; a process not captured by standard laboratory experiments. Thus, warming permafrost soils are not just more rapidly cycling fresh plant litter but losing organic matter that accumulated over decades to millennia.

1. Introduction

Climate change is rapidly transforming the Arctic (Post et al., 2019; Steffen, 2006). Permafrost thaw may facilitate microbial decomposition of vast amounts of soil organic carbon (C) (472 $\pm$ 27 Pg C for 0–1 m) (Hugelius et al., 2014) into the greenhouse gases CO_2 and CH_4 (Schuur et al., 2015), accelerating climate and ecosystem changes. Permafrost temperatures in the northern circumpolar continuous permafrost zone have increased by 0.39 $\pm$ 0.15°C (2007–2016, Biskaborn et al., 2019), concurrent with increases in active layer thickness (*medium confidence*, Meredith et al., 2019). The area underlain by near-surface (within 4 m) permafrost may decrease by 2%–66% (RCP2.6) or 30%–99% (RCP8.5) by 2100, and this loss is projected to release up to 240 Pg C to the atmosphere (Meredith et al., 2019), but the magnitude, timing, and proportions of CH_4 and CO_2 fluxes remain highly uncertain (Schuur et al., 2015; Turetsky et al., 2020).

Non-growing season C emissions are emerging as an important contribution to the annual C balance of Arctic ecosystems (Euskirchen et al., 2012; Fahnestock et al., 1998; Morgner et al., 2010; Oechel et al., 1997; Raz-Yaseef et al., 2017; Watts et al., 2021; Welker et al., 2000, 2004), turning the Arctic into a net C source (Commane et al., 2017; Natali et al., 2019). It remains unclear, however, which soil C pools fuel microbial respiration from fall to spring. Some of this may originate from older C in thawing permafrost, which like fossil fuel combustion, has not participated in the global C cycle for millennia, but may increasingly contribute to land-atmosphere C emissions. Reducing the uncertainty in our understanding of non-growing season emission and the permafrost

C feedback to climate change urgently requires direct, year-round observations of C emissions and sources from permafrost landscapes.

Measurements of the radiocarbon (^{14}C) content of soil-atmosphere C emissions can be used to estimate how rapidly soils may sequester or lose C in response to changes in environmental conditions or net primary productivity (Trumbore, 2006). These data provide an estimate of transit time (the age of C leaving the soil) and can be used to apportion emissions into plant- and microbial contributions and to quantify losses of permafrost C (Estop-Aragonés et al., 2018; Lupascu, Welker, Xu, & Czimczik, 2014; Schuur et al., 2009).

Soil C emissions are a major component of ecosystem C emissions. A significant proportion of soil C emission originates from the rhizosphere, that is, respiration of plant roots and microorganisms that consume root exudates, which have a similar $\Delta^{14}CO_2$ signature to ambient air. Currently (2021), atmospheric $\Delta^{14}CO_2$ is about 0‰ following a 70-year decline of ^{14}C in the atmosphere from a maximum in the 1960s, when testing of thermonuclear weapons resulted in the formation of additional (bomb or modern) ^{14}C that subsequently mixed into the C cycle and became diluted by ^{14}C-free fossil fuel CO_2 emissions (Graven et al., 2020; Levin et al., 2010). Microbial emissions constitute the remainder of the soil C efflux and are either slightly depleted ($\Delta^{14}C < 0$‰, "old") from decomposition of pre-1950 substrate, or enriched ($\Delta^{14}C > 0$‰, "modern") from post-1950 substrate. In permafrost soils, microbial emissions of previously frozen C are strongly ^{14}C-depleted due to radioactive decay ($\Delta^{14}C << 0$‰, "ancient").

Soil C source apportionment studies often combine ^{14}C analysis of ecosystem (or soil), rhizosphere, and microbial emissions ($^{14}CO_{2\,eco}$, $^{14}CO_{2\,rhizo}$, and $^{14}CO_{2\,micro}$, respectively) to determine the relative contribution of rhizosphere (R_{rhizo}) and microbial emissions (R_{micro}) to the total (R_{eco}) (Equations 1 and 2). Ecosystem C emissions are collected in the field, rhizosphere C emissions can be measured by incubating roots or approximated from ^{14}C measurements of atmospheric CO_2, and microbial C emissions from laboratory incubation experiments.

$$f_{eco} = 1 = f_{rhizo} + f_{micro} = \frac{R_{rhizo}}{R_{eco}} + \frac{R_{micro}}{R_{eco}} \tag{1}$$

$$^{14}CO_{2\,eco} = f_{rhizo}\,^{14}CO_{2\,rhizo} + f_{micro}\,^{14}CO_{2\,micro} \tag{2}$$

Past studies have advanced our understanding of soil C emissions and their sources from permafrost soils (Hicks Pries et al., 2013, 2016; Lupascu, Welker, Seibt, et al., 2014; Nowinski et al., 2010; Street et al., 2020) but suffer shortcomings. First, to collect sufficient mass for ^{14}C analysis, common approaches accumulate soil CO_2 in chambers (Lupascu, Welker, Seibt, et al., 2014) and may remove ambient atmospheric CO_2 from the headspace (Czimczik et al., 2006; Hicks Pries et al., 2013; Plaza et al., 2019). Chambers cover the ground for 0.5–48 hr during which the soil CO_2-depth gradient is disturbed. This approach only provides a snapshot of emissions and may miss advective fluxes in response to changes in atmospheric pressure or precipitation events (Lupascu, Welker, Seibt, et al., 2014), and due to the high cost of ^{14}C analysis, most studies collect chamber samples about once a month and few have collected outside the growing season (Lupascu et al., 2018; Winston et al., 1997). Second, the source of microbial C emissions is assessed in incubations (Schädel et al., 2014; Treat et al., 2015) that disrupt the autotroph–heterotroph respiratory continuum (Högberg & Read, 2006). However, we commonly observe a greater range of microbial-respired $^{14}CO_2$ in the field than in laboratory incubation studies (Lupascu, Welker, Seibt, et al., 2014).

As permafrost thaws, it is prudent to investigate the vulnerability of its organic matter to decomposition in situ. Here, we use a recently developed a passive CO_2 sampler (capturing CO_2 by diffusion, Pedron et al., 2021) to collect soil $\Delta^{14}CO_2$ from a graminoid tundra for two years (June 2017–August 2019). These data are then used to apportion soil C emissions into rhizosphere and microbial contributions. The resulting annual $^{14}CO_2$-depth profiles allow us to investigate microbial C sources during the non-growing season. Our approach quantifies the mean age of the land-atmosphere C flux on a monthly to annual scale and provides a basis for a more systematic quantification of permafrost C losses in the rapidly changing Arctic.

2. Materials and Methods

2.1. Field Site and Sample Collection

We continuously captured soil CO_2 for $\Delta^{14}CO_2$ analysis from a moist acidic tussock tundra near Toolik Field Station, AK, USA (68.625478°N, 149.602199°W, 724 m) with passive samplers consisting of permanently
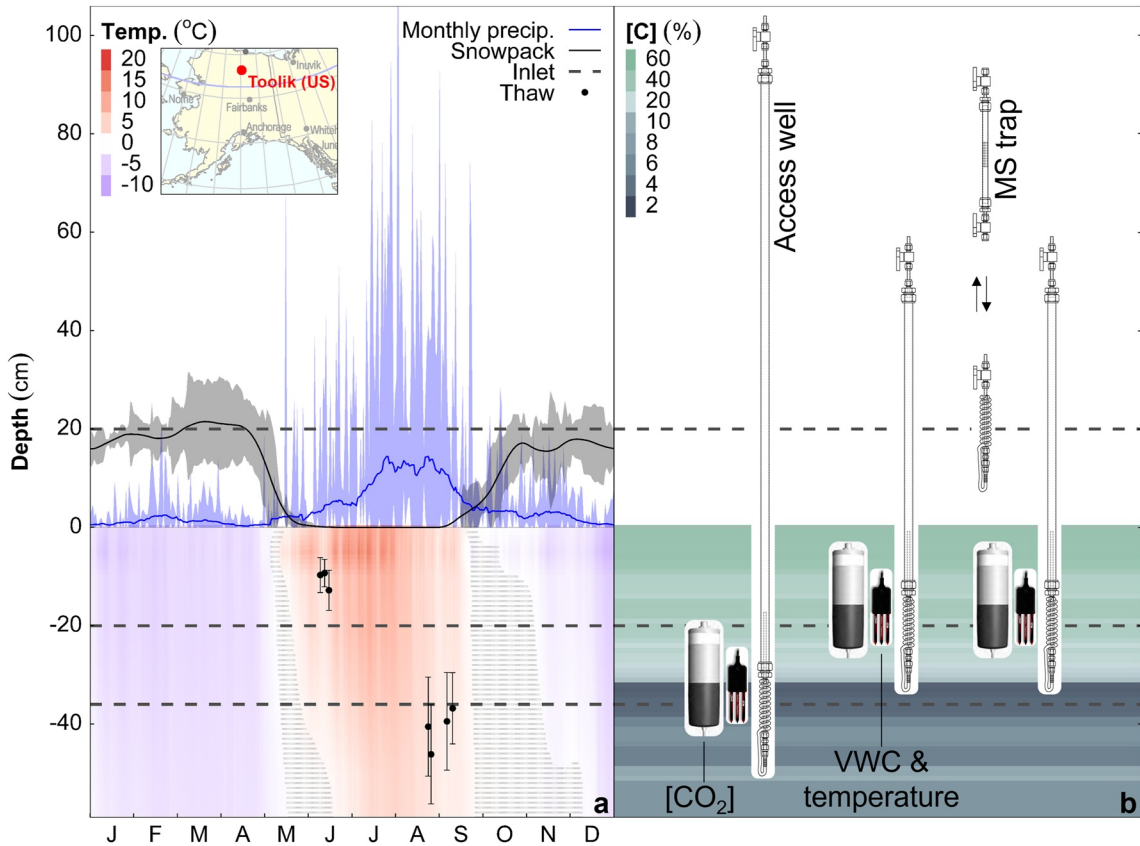
Figure 1. (a) Environmental data during the sampling period (June 2017–September 2019), averaged by day of year and either smoothed (precipitation, snowpack, from Toolik EDC) or modeled from observations (thaw depth). The soil is shaded based on Toolik EDC temperature data, with dots showing zero curtain. (b) Site setup. Permanent access wells attached to exchangeable molecular sieve (MS) traps were suspended above the surface (20 cm, $n = 1$) or buried within the active layer with silicone inlets at −20 (O horizon, $n = 2$ (tussock/swale)) and −36 cm below the surface (A horizon, $n = 1$) alongside $[CO_2]$ and VWC + temperature probes within a 1 m² area in a moist acidic tundra system near Toolik Field Station, AK, USA (68.625478°N, 149.602199°W, 724 m). The soil is shaded by C percent of bulk organic matter (averaged from soil cores) and scaled to distinguish organic (green > 20%) from mineral (blue < 20%) soil.

installed access wells (diffusive silicone tubing inlet attached to steel tubing path) connected to exchangeable evacuated cylinders or molecular CO_2 sieve (MS) traps (Pedron et al., 2021). Access wells were buried within the active layer at 20 cm (O horizon, $n = 1$ each, tussock/swale) and 36 cm (A horizon, $n = 1$) and suspended above the surface (20 cm, $n = 1$), all within a 1-m² area (Figure 1b). Samples were collected from June 2017 to August 2019 over periods of 3–6 weeks using canisters (June 2017–September 2017), MS traps (September 2017–September 2018), and alternating canisters and MS traps (September 2018–August 2019). We also collected high-resolution (<2-week) samples in 0.5 L canisters ($n = 22$, 2017 (June, September, November), $n = 20$, 2018 (March, August), $n = 4$, 2019 (June)).

The data were sequentially corrected for: (a) leakage of ambient air CO_2 into traps or canisters and (b) mixing of ambient air CO_2 into the soil pore space, given the high soil porosity (Hirsch et al., 2004) (Equation 3).

$$^{14}CO_{2\,cor} = \frac{^{14}CO_{2\,spl} - {}^{14}CO_{2\,air} * f_{air}}{1 - f_{air}} \tag{3}$$

where $^{14}CO_{2\,cor}$ and $^{14}CO_{2\,spl}$ represent the corrected or measured $\Delta^{14}CO_2$ of a sample, respectively, f_{air} the proportion of ambient air CO_2, and $^{14}CO_{2\,air}$ the $\Delta^{14}CO_2$ of ambient air.

The proportion of MS trap air-CO_2 from leakage was calculated from extraction of a set of traps that were shipped back and forth from the field site and attached, but never opened to access wells ($n = 8$, 0.16 ± 0.1 ug C d⁻¹). The proportion of air-CO_2 due to soil-air mixing was calculated from the ratio of air $[CO_2]$ to soil $[CO_2]$ at the depth of each inlet, averaged over each sampling period.

We episodically monitored thaw depth with a steel-tipped tile probe in swales, and retrieved continuous environmental data (air and soil temperatures, insolation, precipitation, snow depth) from Toolik's Environmental Data Center (Environmental Data Center Team, 2020) and atmospheric CO_2 concentrations and ecosystem CO_2 fluxes from an eddy covariance (EC) tower at Imnavait Creek (wet sedge tundra, 12 km WSW; Euskirchen et al., 2019). We deployed soil (CO_2) (Carbocap GMP343, 11 June 2017–25 August 2019, 30-s resolution, Vaisala, Finland) and temperature and volumetric water content (VWC) (Decagon 5 TM, 12 September 2017–26 August 2019, 15-min resolution, METER, USA) probes ($n = 3$ of each) with the buried access wells (Figure 1b). Data gaps were filled using day-of-year means over the sampling period (~14% of [CO_2], ~19% of VWC and temperature daily values).

To validate the samplers, we measured ecosystem CO_2 respiration flux (R_{eco}) with traditional dynamic soil chambers installed in June 2017, 10 m away from the access wells. Chamber bases were inserted to 2 cm depth and vegetation was not clipped ($n = 3$ each, tussock/swale). We collected ambient air CO_2 and chamber R_{eco} samples for isotopic analysis in June, September, & November 2017 ($n = 37$), March & August 2018 ($n = 11$), and August 2019 ($n = 2$), and measured R_{eco} rate in June and September 2017 ($n = 39$; Lupascu, Welker, Seibt, et al., 2014, 2018).

Growing season chambers were flushed with ambient air before being attached to bases, and isotopes were subsequently corrected for air volume. Chambers sampled in November 2017 ($n = 3$) were left attached to bases at the end of the 2017 growing season, with Bev-A-Line tubing connected to a central point, accessible above snowpack. We flushed their headspace CO_2 with ambient air and sampled after 24 hr of accumulation, thereby minimizing contamination from prior accumulation.

To sample CO_2 for isotope analyses, we left the growing season chambers closed until the CO_2 concentration inside the chamber was at least double that of ambient air (up to 24 hr). After measuring its concentration, the CO_2 was dried (Drierite, W.A. Hammond Drierite Co. Ltd., Xenia, OH, USA) and collected onto u-shaped MS traps ("u-traps," 2 g of powder-free 13X 8 × 12 beads, Grace, USA) by recirculating the headspace air at a rate of 0.5 L min^{-1} for 15 min. These MS u-traps used to collect chamber or ambient air CO_2 are distinct from the MS traps previously described in both shape (u-shaped vs. straight) and MS dimension (8 × 12 beads vs. 45–60 mesh) but operate by the same principle of size-selective molecule retention. These data were corrected for mixing of ambient air CO_2 (Equation 3), where the fraction of air-CO_2 was calculated from ratio of air [CO_2] to chamber-headspace [CO_2]. Isotope data with a calculated fraction of air >40% ($n = 23$, 47% of samples) were likely affected by leakage around the chamber base – a common issue in organic soils and tussock/swale terrain affected by freeze-thaw cycles – and excluded from results.

Growing season R_{eco} fluxes were quantified with an infrared gas analyzer and data logger (LI-840, LI-1400, LI-COR Biosciences, Lincoln, NE, USA) at a rate of 0.5 L min^{-1}. Emission rates were calculated from the slope of time versus CO_2 concentration curves using linear regression. Winter fluxes were not calculated because accumulating enough headspace CO_2 for ^{14}C analysis disturbed the soil CO_2 gradient and saturated the headspace, yielding small fluxes with large uncertainties.

We collected soil samples for incubations and bulk soil analyses by cutting rectangular columns of soil from 6 m south of the samplers with either a saw ($n = 1$ each tussock/swale in thawed soil, September 2017) or electric chainsaw ($n = 1$ each tussock/swale in frozen soil, March 2018). Cylindrical cores collected by powered corer ($n = 3$, 2015) and a modified rotary hole saw ($n = 2$, 2019) from a nearby site (moist acidic tussock tundra, <1 km away) were also used after comparison of bulk soil isotopes revealed no significant differences (all 2-sample Student's t-test $p > 0.05$ for 10-cm depth bins). Soils were stored frozen in plastic freezer bags.

2.2. Laboratory Analyses

At UC Irvine, CO_2 was thermally desorbed from u-traps and MS traps (Pedron et al., 2021) or extracted from canisters (Lupascu, Welker, Seibt, et al., 2014) on a vacuum line and converted to graphite using a sealed-tube zinc reduction method (Xu et al., 2007). Graphite was analyzed for $\Delta^{14}C$ with accelerator mass spectrometry (NEC 0.5 MV 1.5SDH-2 AMS) alongside processing standards and blanks with a measurement uncertainty of <3‰ (Beverly et al., 2010).

Soil cores were separated into organic or mineral soil and sectioned into intervals (1.5–14 cm) while frozen. For bulk soil analysis, soil was dried at 60°C to constant mass, weighed, and ground to powder using rotary blade and ball mills for organic and mineral soils, respectively. For $\Delta^{14}C$ analysis, samples were combusted in pre-combusted, evacuated quartz tubes with cupric oxide (900°C, 3 hr) and the resulting CO_2 processed as described above. Bulk soil C was measured alongside processing standards and blanks with EA-IRMS (Fisons NA-1500NC, DeltaPlus XL, Thermo, USA).

Incubations (2–158 g soil) were performed on field-moist samples at 22, 7, and −20°C in glass mason jars (0.5–2 L) flushed with CO_2-free air and kept in the dark. CO_2 concentrations were measured periodically with a LI-COR 820, and the respired CO_2 was extracted and converted to graphite as described above once concentrations reached 30% (17–49 days). Short (~1-day) incubations were also performed on roots harvested from the September 2017 soil cores on the same day of collection to quantify rhizosphere emissions. These data provided predictive relationships between microbial CO_2 emissions (R_{micro}), depth, and temperature.

3. Data Processing and Soil C Emission Partitioning

Using the data collected during the 2-year study period, we averaged meteorological, soil $[CO_2]$, temperature, VWC, and access well $\Delta^{14}CO_2$ data month to month over one year. Access well aggregates were weighted by the period overlapping the beginning and end of each timestep. To account for our 2–6-week sampling periods and data gaps, we chose to represent out data products at calendar month resolution. We found no significant differences in soil $\Delta^{14}CO_2$ collected at 20 cm depth under tussock or swale (paired two-tailed t-test p-value >> 0.05).

The steps and assumptions used to determine a surface isotopic flux are detailed in the Supplement (S) and shown conceptually in Figure S5 of Supporting Information S1. We created a monthly $\Delta^{14}CO_{2\,eco}$-depth model using measured predictors along depth (bulk soil $\Delta^{14}C$) and time (days snow-free, days snow-covered) from the deepest inlet depth (−36 cm) to the organic soil surface (0 cm). Model details are described in S: *Multivariate adaptive regression splines*, and results in Table S2 and Figure S8 in the Supporting Information S1.

We used our incubation results with the field temperature data to model microbial respiration at each depth. R_{micro} CO_2 flux at individual depths were modeled (Table S1, Figures S6a, and S6c in Supporting Information S1) from laboratory soil incubations as an exponentially decaying nonlinear least squares fit (R *nls* function) of temperature and depth (Equation 4):

$$R_{micro} = a * \exp(b * \text{Temperature} + c * \text{Depth}) \tag{4}$$

The model was weighted by the inverse square of the incubation flux standard error (error bars in Figure S6a in Supporting Information S1). Model error predictions were calculated from Monte Carlo simulation of confidence intervals (R *predictNLS v1.0-4*), which allows the construction of more realistic estimates of nonlinear models than a first-order Taylor expansion (simple linearization) approach. This approach may also consider uncertainties in a predictor value, allowing us to propagate the standard error of empirical temperature (0.11°C in June at 0 cm to 0.0009°C in September at −20 cm, Figure S6d in Supporting Information S1) into the model results. This yields R_{micro} errors (Figure S6e in Supporting Information S1) which are greatest in the shallow soil during summer (when R_{micro} is also maximal), on average 16% ± 4% of R_{micro} (mean ± sd, $n = 120$ at monthly resolution).

Summing the column values at each timestep allowed us to estimate the contribution of R_{micro} to R_{eco} surface emissions for a temporal partitioning of f_{micro} versus f_{rhizo} (Equation 1). Model details are further described in S: *Non-linear least squares*, and results in Table S1 and Figure S6 in Supporting Information S1. Applying this partitioning to our modeled $^{14}CO_{2\,eco}$ at each depth (Equation 2), we calculated $^{14}CO_{2\,micro}$. The column $^{14}CO_2$ value (i.e., the surface signature) is the sum of a flux-weighted multi-endmember mixing model at every timestep, where each discrete depth is an endmember. We used Point Barrow air ($\Delta^{14}C = 4.2 \pm 3.7$ mean ± sd over the sampling period) for $^{14}CO_{2\,rhizo}$ (Xiaomei Xu, pers. com.). Considering the fully partitioned column respiration relative to the $\Delta^{14}C$ of the available substrate, we finally deduced the fraction and magnitude of R_{micro} derived from either permafrost (with bulk soil ^{14}C at the bottom of the active layer) or recently assimilated soil organic matter (with bulk soil ^{14}C at the top of the active layer).
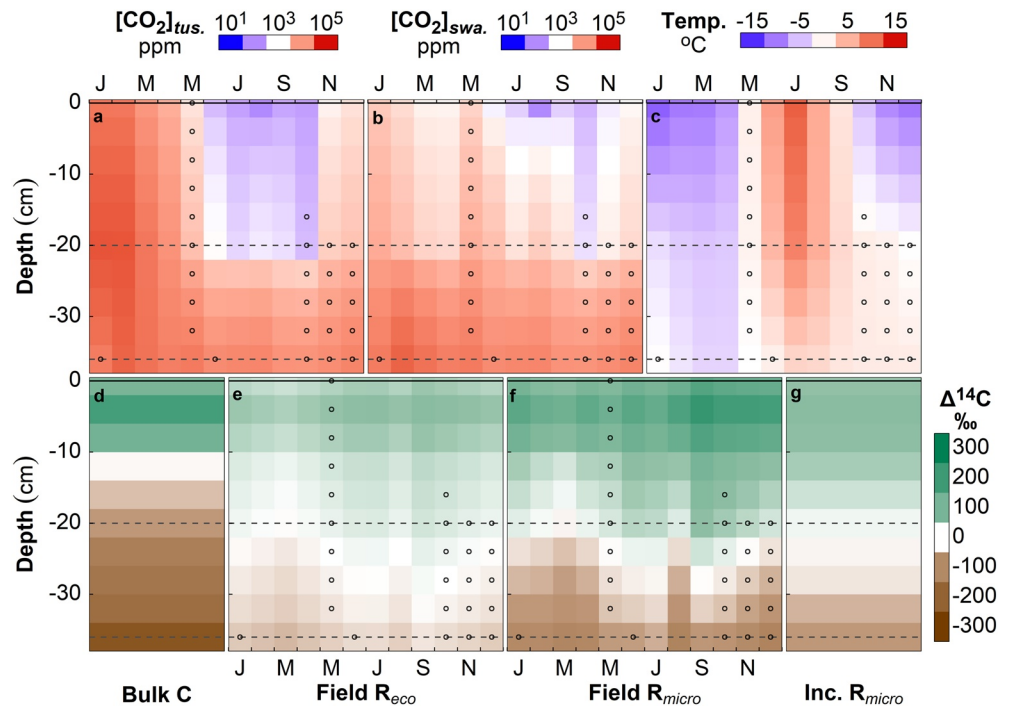
Figure 2. Upper panels (a–c) show linear interpolations of month of year mean values of environmental data from in situ probes. Surface values for $[CO_2]$ and temperature were taken from Imnavait Fen EC tower and Toolik EDC, respectively. Bottom panels compare $\Delta^{14}C$ of (d) bulk soil organic matter, (e) soil CO_2 modeled from (d) and passive sampler observations, (f) microbial CO_2 derived from (e) using temperature-dependent emissions partitioning, and (g) microbial CO_2 from incubations a function of depth (0 cm = top of O horizon) and month of year. *Dashed horizontal lines* show access well inlet depths while *open dots* show zero curtain.

4. Results and Discussion

4.1. Bulk Soil Properties

The active layer mineral soil is a mottled silt loam (1.0%–19% C, 0.06%–1.1% N) overlain by a 20-cm thick organic layer (21%–46% C, 0.52%–2.8% N) (Figures 1b, S1c, and S1d in Supporting Information S1). As expected for cryoturbated and hummocky terrain, the bulk density increases with depth, yet is highly variable (0.12–2.1 g cm^3 mineral, 0.008–0.38 g cm^3 organic; Figure S1b in Supporting Information S1). Seasonal thaw depth varies from 2 to 73 cm (Figure 1a, 2017–2019), with a maximum in August. Linear models of two local records for August indicate regional active layer deepening (CALM U12 A: 6.8 ± 1.4 cm, 1995–2020; LTER 1989 Moist Acidic Tussock: 7.1 ± 3.3 cm, 1993–2016; prediction changes ±se, with both $p < 0.001$), even though no significant trend has been documented for annual air temperatures (Bieniek et al., 2015; Cherry et al., 2014).

The mean age of the bulk organic matter increases with depth from modern ($\Delta^{14}C \geq 0‰$; organic material deposited/formed after 1950) to approximately 2,000 years BP at about 40 cm depth (Figures 2d and S1e in Supporting Information S1). The bomb-spike is apparent at 5–10 cm depth, indicating organic material formed during the mid-20th century. Consistent with previous work (Lupascu et al., 2018), microbially-respired CO_2 captured by incubation follows a similar trend with depth (Figures 2g and S1e in the Supporting Information S1), but is consistently younger than bulk C (enriched or depleted relative to old ($\Delta^{14}C < 0‰$) or modern ($\Delta^{14}C > 0‰$) bulk C, respectively) at the same depths and for the same cores – reflecting preferential microbial consumption of younger organic matter.

4.2. Seasonal Patterns in Soil Temperature, Moisture, and CO_2

Zero curtain conditions, during which soil temperatures remain near 0°C, were present for 168 days (8 May–26 June, 21 September–17 January from day of year in situ temperature sensor means above 36 cm depth) (Figure 2c).
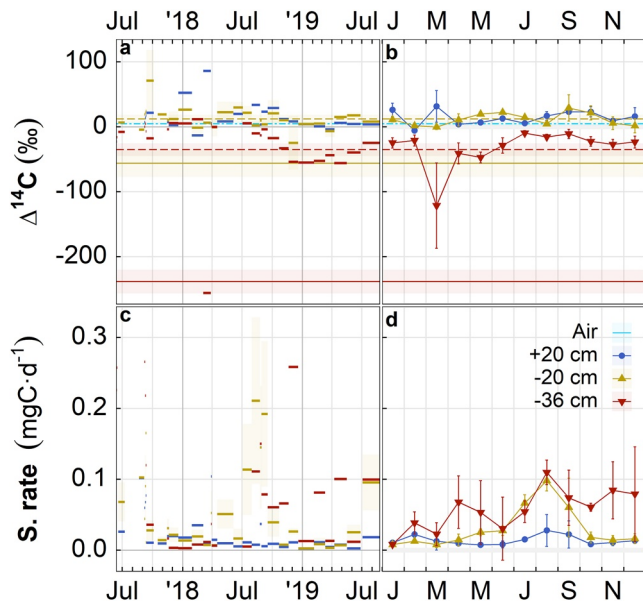
Figure 3. Time series of process-blank corrected (a) $\Delta^{14}C$ and (c) sampling rate of soil CO_2 in graminoid tundra (June 2017–September 2019). Horizontal segments span collection dates for each sample. The *horizontal dot-dash line* indicates the mean $\Delta^{14}CO_2$ in ambient air, *dashed lines* $\Delta^{14}CO_2$ emitted from microbial respiration during laboratory incubations of soils collected within ± 6 cm of inlets, and *solid lines* $\Delta^{14}C$ of the bulk soil. Shading around lines and segments shows standard error. Panels (b and d) show the same data as (a and c), respectively, averaged by month of year and weighted by sample period within month with standard error bars.

Zero curtain conditions are associated with significant C losses from Arctic ecosystems (Zona et al., 2016) and fall and winter are emerging as critical periods for the annual C budget of the Arctic (Commane et al., 2017; Natali et al., 2019; Oechel et al., 2014). Here we show that the zero curtain remained open through mid-January, confirming previous observations of a 1–2 months longer than expected period of zero curtain conditions and C loss by Arndt et al. (2019).

CO_2 concentrations significantly differed seasonally and with the micro-terrain (Figures 2a and 2b). During the growing season, CO_2 concentration increased with increasing depth. Concentrations were uniform within the mineral soil, but lower in tussocks than swales, where the soil was denser, moister (Figure S3c in Supporting Information S1), and less exposed to wind. From fall to late winter (January–February), CO_2 concentrations in the top soil increased, indicating the trapping of CO_2 under the snowpack as well as a reduction in pore space volume and connectivity. Concentrations were greater in tussocks, where the CO_2-depth gradient was reversed. This might indicate lateral flow and accumulation of CO_2 under tussocks. In spring, CO_2 concentrations were lower and more uniform, possibly due to the formation of deep cracks, ventilation events, and diminishing biological activity at low temperatures (Figures 2c and S3e in Supporting Information S1).

While the observed CO_2 concentrations allowed us to validate our $^{14}CO_2$ collection rates (Figure 3c), they were were not suitable for estimating surface fluxes during periods of snow-cover because gradient methods assume a linear increase of CO_2 with depth. Thus, we relied on nearby eddy covariance data to estimate surface fluxes (Figure 4).

4.3. Seasonal Patterns in the Age of R_{eco}

Year-round collection of soil $\Delta^{14}CO_2$ revealed a spatial correlation to depth, as well as depth-dependent seasonality (Figures 3a and 3b). These trends are further illustrated using our depth-resolved monthly model of the data (Figures 2e and S8 in Supporting Information S1; $R^2 = 0.82$). CO_2 captured near the surface is always younger than at depth, with the −20 cm inlet typically capturing bomb-C ($\Delta^{14}C > 0$) and the −36 cm inlet aged C, which is characteristic of soils developing in stable landscapes (Shi et al., 2020).

The age of soil CO_2 changes significantly throughout the year (Figure 2e). During the growing-season, the oldest CO_2 is respired at depth during maximum thaw, temperature (Figure 2c), and CO_2 production (Figures 2a and 2b), and is significantly younger than bulk soil C. This confirms previous observations (Czimczik & Welker, 2010; Czimczik et al., 2006; Lupascu, Welker, Seibt, et al., 2014) indicating that summer CO_2 production is fueled to a considerable extent by recent plant assimilates. Moreover soil $\Delta^{14}CO_2$ resembles $\Delta^{14}CO_2$ produced in incubations of soil segments within ± 6 cm of each inlet (Figures 2e and 2g). This suggests that short-term incubations capture the typical growing season average of microbial C sources.

From fall and throughout the non-growing season (September–March), soil $\Delta^{14}CO_2$ at each depth becomes older (Figure 2e). At 20 cm depth, we recover soil CO_2 that is ^{14}C-enriched ($\Delta^{14}CO_2 > 0\permil$) relative to CO_2 in ambient air at the end of the growing season and becomes ^{14}C-depleted ($\Delta^{14}CO_2 < 0\permil$) throughout the winter. This pattern is amplified at 36 cm depth. Seasonal trends for CO_2 captured from the above-surface inlet are similar to those at 20 cm depth.

Our continuous observations uncovered a large seasonal variation in soil $\Delta^{14}CO_2$, with older C pools fueling CO_2 production during the non-growing season. This shift in $^{14}CO_2$, combined with the increase in soil $[CO_2]$ during the zero-curtain period demonstrates that microbial CO_2 production persists through the fall and into the winter. Thus, our work provides further evidence that non-growing season emissions contribute significantly to the loss of older soil C pools from warming permafrost soils (Commane et al., 2017; Natali et al., 2019).
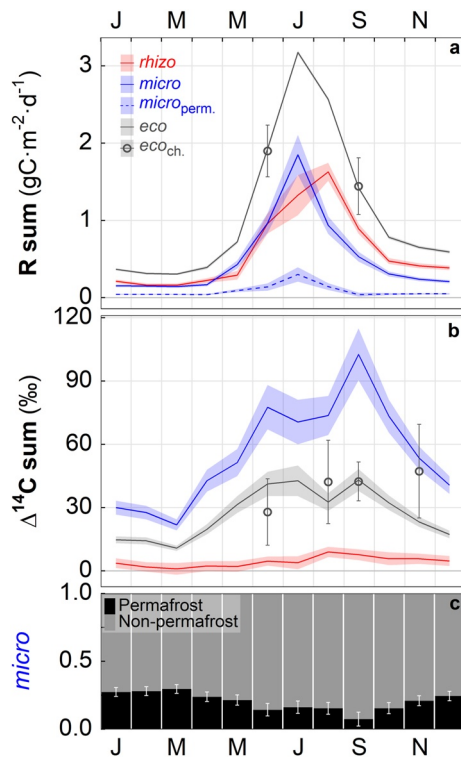
Figure 4. Flux (a) and $\Delta^{14}C$ (b) of total surface CO_2 emissions (R_{eco}) and contributions from the rhizosphere (R_{rhizo}, $\Delta^{14}C$ is barrow air) and decomposition of organic matter by heterotrophic microorganisms (R_{micro}). The permafrost-derived portion of R_{micro} (c) is also shown as a dashed line in (a). Circles show month of year chamber mean, and all error indicators (bands and bars) show 95% CI.

4.4. Microbial C Sources

Previous studies conducted during the growing season (Czimczik & Welker, 2010; Czimczik et al., 2006; Hicks Pries et al., 2016; Schuur & Trumbore, 2006; Schuur et al., 2009) used incubations to estimate microbial contributions to R_{eco} fluxes. Our results (Figures 2f and 2g) show that this approach is a reasonable representation of microbial C sources during the growing season.

However, we find that the range of microbial $\Delta^{14}CO_2$ outside the growing season exceeds that observed during our incubation experiments. The age of microbial CO_2 in the field is frequently older than that of any CO_2 captured by incubations. In early fall, the presence of older CO_2 may result from the sampler capturing CO_2 originating below it and diffusing upwards. As the active layer refreezes, it is more likely that the older CO_2 originates from the decomposition of locally available, older material. We find that the microbial $\Delta^{14}CO_2$ approaches $\Delta^{14}C$ of the bulk C (Figure 2d).

Our results demonstrate that short-term incubation experiments do not capture the full range of C sources utilized by soil microorganisms in soils and support the emerging view of a plant-microbe-soil continuum (Högberg & Read, 2006; Sokol et al., 2019) and of dissolved organic matter as a source of microbial C and energy (Roth et al., 2019). Our data suggest that microorganisms rely increasingly on local C sources in fall and winter as they become disconnected from fresh plant exudates and other mobile C sources. Hence, we can expect climate change, via warmer soil temperatures and active layer deepening, to accelerate the loss of older C from permafrost soils during the polar night. This CO_2 injection of slowly-accumulated soil C pools into the modern atmosphere has the potential to amplify climate warming, leading to more permafrost thaw and more ancient C emissions in the near future.

4.5. Microbial C Contributions to R_{eco}

Ecosystem and microbial respiration in Arctic tundra follow a temperature-dependent seasonal dynamic and are greatest during the growing season, with a maximum in July (Figure 4a). We estimate that microbial contributions ranged from 35% to 60% of R_{eco} ($f_{micro} = 58\%$, Figure S7 in Supporting Information S1). The annual column flux-weighted mean $\Delta^{14}CO_2$ values of ecosystem and microbial respiration were $34 \pm 10\text{‰}$ and $68 \pm 20\text{‰}$ mean $\pm$ se, respectively (Figure 4b). Column $\Delta^{14}CO_2$ $_{eco}$ was not significantly different from the growing season chamber $\Delta^{14}CO_2$ $_{eco}$ (one sample t-test p-value = 0.58, overlapping 95% CI in Figure 4b).

Our continuous observations of soil and ecosystem $\Delta^{14}CO_2$ provide unprecedented insight to microbial C sources and enable a more systematic observation of C cycling in Arctic soils by quantifying the loss of ancient permafrost C from thawing permafrost. We find that the oldest (and greatest magnitude of) microbially derived C is produced in mid-summer, but that these emissions are masked by the greater magnitude of respiration in the organic horizons. We show for the first time that non-growing season C emissions are fueled by older C pools, with the greatest relative contribution of permafrost C to microbial (and ecosystem) emissions in fall and winter. Under current conditions, non-growing season microbial emissions accounted for $18\% \pm 6\%$ (mean $\pm$ se) of annual soil C emissions, $22\% \pm 2\%$ of which were derived from permafrost C.

5. Conclusions

We combine year-round observations of soil $\Delta^{14}CO_2$ in Arctic graminoid tundra with incubation experiments and bulk soil analyses to reveal seasonally dynamic microbial C sources. We show that microbial C emissions during the non-growing season are fueled by older soil C pools and further highlight the polar night as a critical period for climate-vulnerable permafrost C pools.

Data Availability Statement

Data from the Arctic Observatory Network Imnavait Creek Fen eddy covariance tower (2017–2019) were used to create this manuscript (Euskirchen et al., 2017). Data from Toolik Field Station Environmental Data Center abiotic monitoring were also used (Environmental Data Center Team, 2020). Figures and models were made with *R* version 4.0.3: https://cran.r-project.org/bin/windows/base/old/. The R_{micro} model was created with *R nls* function from the base *R* stats package version 3.6.2. The $\Delta^{14}C_{eco}$ model was created with the *R earth* package, that builds multivariate regression models (Friedman, 1991). Compiled sensory data and thaw depth observations are available in the Arctic Data Center repositories: https://doi.org/10.18739/A2Q814S37; https://doi.org/10.18739/A2V11VK6H; and https://doi.org/10.18739/A2930NV02.

References

Arndt, K. A., Oechel, W. C., Goodrich, J. P., Bailey, B. A., Kalhori, A., Hashemi, J., et al. (2019). Sensitivity of methane emissions to later soil freezing in Arctic tundra ecosystems. *Journal of Geophysical Research: Biogeosciences*, *124*(8), 2595–2609. https://doi.org/10.1029/2019JG005242

Beverly, R. K., Beaumont, W., Tauz, D., Ormsby, K. M., von Reden, K. F., Santos, G. M., et al. (2010). The Keck carbon cycle AMS laboratory, University of California, Irvine: Status report. *Radiocarbon*, *52*(2), 301–309. https://doi.org/10.1017/S0033822200045343

Bieniek, P. A., Bhatt, U. S., Walker, D. A., Raynolds, M. K., Comiso, J. C., Epstein, H. E., et al. (2015). Climate drivers linked to changing seasonality of Alaska coastal tundra vegetation productivity. *Earth Interactions*, *19*(19), 1–29. https://doi.org/10.1175/EI-D-15-0013.1

Biskaborn, B. K., Smith, S. L., Noetzli, J., Matthes, H., Vieira, G., Streletskiy, D. A., et al. (2019). Permafrost is warming at a global scale. *Nature Communications*, *10*(264), 1–11. https://doi.org/10.1038/s41467-018-08240-4

Cherry, J. E., Déry, S. J., Cheng, Y., Stieglitz, M., Jacobs, A. S., & Pan, F. (2014). Climate and hydrometeorology of the Toolik lake region and the Kuparuk river basin: Past, present, and future. In *Alaska's changing Arctic* (pp. 31–60). Oxford University Press.

Commane, R., Lindaas, J., Benmergui, J., Luus, K. A., Chang, R. Y.-W., Daube, B. C., et al. (2017). Carbon dioxide sources from Alaska driven by increasing early winter respiration from Arctic tundra. *Proceedings of the National Academy of Sciences of the United States of America*, *114*(21), 5361–5366. https://doi.org/10.1073/pnas.1618567114

Czimczik, C. I., Trumbore, S. E., Carbone, M. S., & Winston, G. C. (2006). Changing sources of soil respiration with time since fire in a boreal forest. *Global Change Biology*, *12*(6), 957–971. https://doi.org/10.1111/j.1365-2486.2006.01107.x

Czimczik, C. I., & Welker, J. M. (2010). Radiocarbon content of CO_2 respired from high arctic tundra in Northwest Greenland. *Arctic Antarctic and Alpine Research*, *42*(3), 342–350. https://doi.org/10.1657/1938-4246-42.3.342

Environmental Data Center Team. (2020). *Meteorological monitoring program at Toolik*. Toolik Field Station; Institute of Arctic Biology; University of Alaska Fairbanks. Retrieved from https://www.uaf.edu/toolik/edc/monitoring/abiotic/met-data-query.php

Estop-Aragonés, C., Czimczik, C. I., Heffernan, L., Gibson, C., Walker, J. C., Xu, X., & Olefeldt, D. (2018). Respiration of aged soil carbon during fall in permafrost peatlands enhanced by active layer deepening following wildfire but limited following thermokarst. *Environmental Research Letters*, *13*(8), 85002. https://doi.org/10.1088/1748-9326/aad5f0

Euskirchen, E. S., Bret-Harte, M. S., Scott, G. J., Edgar, C. W., & Shaver, G. R. (2012). Seasonal patterns of carbon dioxide and water fluxes in three representative tundra ecosystems in northern Alaska. *Ecosphere*, *3*(1), 1–19. https://doi.org/10.1890/ES11-00202.1

Euskirchen, E. S., Bret-Harte, M. S., Shaver, G. R., Edgar, C. W., & Romanovsky, V. E. (2017). Long-term release of carbon dioxide from Arctic tundra ecosystems in Alaska. *Ecosystems*, *20*(5), 960–974. https://doi.org/10.1007/s10021-016-0085-9

Euskirchen, E. S., Bret-Harte, M. S., Shaver, G. R., Edgar, C. W., & Romanovsky, V. E. (2019). *Arctic Observatory Network: Imnavait fen eddy covariance*. Arctic Observatory Network. http://aon.iab.uaf.edu/data_access

Fahnestock, J. T., Jones, M. H., Brooks, P. D., Walker, D. A., & Welker, J. M. (1998). Winter and early spring CO_2 efflux from tundra communities of northern Alaska. *Journal of Geophysical Research*, *103*(D22), 23–27. https://doi.org/10.1029/98JD00805

Friedman, J. H. (1991). Multivariate adaptive regression splines. *Annals of Statistics*, *19*(1), 1–67. https://doi.org/10.1214/AOS/1176347963

Graven, H., Keeling, R. F., & Rogelj, J. (2020). Changes to carbon isotopes in atmospheric CO_2 over the industrial era and into the future. *Global Biogeochemical Cycles*, *34*(11), e2019GB006170. https://doi.org/10.1029/2019GB006170

Hicks Pries, C. E., Schuur, E. A. G., & Crummer, K. G. (2013). Thawing permafrost increases old soil and autotrophic respiration in tundra: Partitioning ecosystem respiration using $\delta^{13}C$ and $\Delta^{14}C$. *Global Change Biology*, *19*(2), 649–661. https://doi.org/10.1111/gcb.12058

Hicks Pries, C. E., Schuur, E. A. G., Natali, S. M., & Crummer, K. G. (2016). Old soil carbon losses increase with ecosystem respiration in experimentally thawed tundra. *Nature Climate Change*, *6*(2), 214–218. https://doi.org/10.1038/nclimate2830

Hirsch, A. I., Trumbore, S. E. ., & Goulden, M. L. (2004). The surface CO_2 gradient and pore-space storage flux in a high-porosity litter layer. *Tellus B: Chemical and Physical Meteorology*, *56*(4), 312–321. https://doi.org/10.3402/tellusb.v56i4.16449

Högberg, P., & Read, D. J. (2006). Towards a more plant physiological perspective on soil ecology. *Trends in Ecology & Evolution*, *21*(10), 548–554. https://doi.org/10.1016/j.tree.2006.06.004

Hugelius, G., Strauss, J., Zubrzycki, S., Harden, J. W., Schuur, E. A. G., Ping, C. L., et al. (2014). Estimated stocks of circumpolar permafrost carbon with quantified uncertainty ranges and identified data gaps. *Biogeosciences*, *11*(23), 6573–6593. https://doi.org/10.5194/bg-11-6573-2014

Levin, I., Naegler, T., Kromer, B., Diehl, M., Francey, R. J., Gomez-Pelaez, A. J., et al. (2010). Observations and modelling of the global distribution and long-term trend of atmospheric $^{14}CO_2$. *Tellus B: Chemical and Physical Meteorology*, *62*(1), 26–46. https://doi.org/10.1111/j.1600-0889.2009.00446.x

Lupascu, M., Czimczik, C. I., Welker, M. C., Ziolkowski, L. A., Cooper, E. J., & Welker, J. M. (2018). Winter ecosystem respiration and sources of CO_2 from the High Arctic tundra of Svalbard: Response to a deeper snow experiment. *Journal of Geophysical Research: Biogeosciences*, *123*(8), 2627–2642. https://doi.org/10.1029/2018JG004396

Lupascu, M., Welker, J. M., Seibt, U., Xu, X., Velicogna, I., Lindsey, D. S., & Czimczik, C. I. (2014). The amount and timing of precipitation control the magnitude, seasonality and sources (^{14}C) of ecosystem respiration in a polar semi-desert, northwestern Greenland. *Biogeosciences*, *11*(16), 4289–4304. https://doi.org/10.5194/bg-11-4289-2014

Lupascu, M., Welker, J. M., Xu, X., & Czimczik, C. I. (2014). Rates and radiocarbon content of summer ecosystem respiration in response to long-term deeper snow in the High Arctic of NW Greenland. *Journal of Geophysical Research: Biogeosciences*, *119*(6), 1180–1194. https://doi.org/10.1002/2013JG002494

Meredith, M., Sommerkorn, M., Cassotta, S., Derksen, C., Ekaykin, A., Hollowed, A., et al. (2019). Chapter 3: Polar regions. *IPCC special report on the ocean and cryosphere in a changing climate*.

Morgner, E., Elberling, B., Strebel, D., & Cooper, E. J. (2010). The importance of winter in annual ecosystem respiration in the High Arctic: Effects of snow depth in two vegetation types. *Polar Research*, *29*(1), 58–74. https://doi.org/10.1111/j.1751-8369.2010.00151.x

Natali, S. M., Watts, J. D., Rogers, B. M., Potter, S., Ludwig, S. M., Selbmann, A. K., et al. (2019). Large loss of CO_2 in winter observed across the northern permafrost region. *Nature Climate Change*, *9*(11), 852–857. https://doi.org/10.1038/s41558-019-0592-8

Nowinski, N. S., Taneva, L., Trumbore, S. E., & Welker, J. M. (2010). Decomposition of old organic matter as a result of deeper active layers in a snow depth manipulation experiment. *Oecologia*, *163*(3), 785–792. https://doi.org/10.1007/s00442-009-1556-x

Oechel, W. C., Laskowski, C. A., Burba, G., Gioli, B., & Kalhori, A. A. M. (2014). Annual patterns and budget of CO_2 flux in an Arctic tussock tundra ecosystem. *Journal of Geophysical Research: Biogeosciences*, *119*(3), 323–339. https://doi.org/10.1002/2013JG002431

Oechel, W. C., Vourlitis, G., & Hastings, S. J. (1997). Cold season CO_2 emission from Arctic soils. *Global Biogeochemical Cycles*, *11*(2), 163–172. https://doi.org/10.1029/96gb03035

Pedron, S., Xu, X., Walker, J. C., Ferguson, J. C., Jespersen, R. G., Welker, J. M., et al. (2021). Time-integrated collection of CO_2 for ^{14}C analysis from soils. *Radiocarbon*, *63*(4), 1303–1319. https://doi.org/10.1017/RDC.2021.42

Plaza, C., Pegoraro, E., Bracho, R., Celis, G., Crummer, K. G., Hutchings, J. A., et al. (2019). Direct observation of permafrost degradation and rapid soil carbon loss in tundra. *Nature Geoscience*, *12*(8), 627–631. https://doi.org/10.1038/s41561-019-0387-6

Post, E., Alley, R. B., Christensen, T. R., Macias-Fauria, M., Forbes, B. C., Gooseff, M. N., et al. (2019). The polar regions in a 2°C warmer world. *Science Advances*, *5*(12), eaaw9883. https://doi.org/10.1126/sciadv.aaw9883

Raz-Yaseef, N., Torn, M. S., Wu, Y., Billesbach, D. P., Liljedahl, A. K., Kneafsey, T. J., et al. (2017). Large CO_2 and CH_4 emissions from polygonal tundra during spring thaw in northern Alaska. *Geophysical Research Letters*, *44*, 504–513. https://doi.org/10.1002/2016GL071220

Roth, V. N., Lange, M., Simon, C., Hertkorn, N., Bucher, S., Goodall, T., et al. (2019). Persistence of dissolved organic matter explained by molecular changes during its passage through soil. *Nature Geoscience*, *12*(9), 755–761. https://doi.org/10.1038/s41561-019-0417-4

Schädel, C., Schuur, E. A. G., Bracho, R., Elberling, B., Knoblauch, C., Lee, H., et al. (2014). Circumpolar assessment of permafrost C quality and its vulnerability over time using long-term incubation data. *Global Change Biology*, *20*(2), 641–652. https://doi.org/10.1111/gcb.12417

Schuur, E. A. G., McGuire, A. D., Schädel, C., Grosse, G., Harden, J. W., Hayes, D. J., et al. (2015). Climate change and the permafrost carbon feedback. *Nature*, *520*(7546), 171–179. https://doi.org/10.1038/nature14338

Schuur, E. A. G., & Trumbore, S. E. (2006). Partitioning sources of soil respiration in boreal black spruce forest using radiocarbon. *Global Change Biology*, *12*(2), 165–176. https://doi.org/10.1111/j.1365-2486.2005.01066.x

Schuur, E. A. G., Vogel, J. G., Crummer, K. G., Lee, H., Sickman, J. O., & Osterkamp, T. E. (2009). The effect of permafrost thaw on old carbon release and net carbon exchange from tundra. *Nature*, *459*(7246), 556–559. https://doi.org/10.1038/nature08031

Shi, Z., Allison, S. D., He, Y., Levine, P. A., Hoyt, A. M., Beem-Miller, J., et al. (2020). The age distribution of global soil carbon inferred from radiocarbon measurements. *Nature Geoscience*, *13*(8), 555–559. https://doi.org/10.1038/s41561-020-0596-z

Sokol, N. W., Kuebbing, S. E., Karlsen-Ayala, E., & Bradford, M. A. (2019). Evidence for the primacy of living root inputs, not root or shoot litter, in forming soil organic carbon. *New Phytologist*, *221*(1), 233–246. https://doi.org/10.1111/nph.15361

Steffen, W. (2006). The Arctic in an Earth system context: From brake to accelerator of change. *Ambio*, *35*, 153–159. https://doi.org/10.1579/0044-7447(2006)35[153:taiaes]2.0.co;2

Street, L. E., Garnett, M. H., Subke, J. A., Baxter, R., Dean, J. F., & Wookey, P. A. (2020). Plant carbon allocation drives turnover of old soil organic matter in permafrost tundra soils. *Global Change Biology*, *26*(8), 4559–4571. https://doi.org/10.1111/gcb.15134

Treat, C. C., Natali, S. M., Ernakovich, J., Iversen, C. M., Lupascu, M., Mcguire, A. D., et al. (2015). A pan-Arctic synthesis of CH_4 and CO_2 production from anoxic soil incubations. *Global Change Biology*, *21*(7), 2787–2803. https://doi.org/10.1111/gcb.12875

Trumbore, S. E. (2006). Carbon respired by terrestrial ecosystems - Recent progress and challenges. *Global Change Biology*, *12*(2), 141–153. https://doi.org/10.1111/j.1365-2486.2006.01067.x

Turetsky, M. R., Abbott, B. W., Jones, M. C., Anthony, K. W., Olefeldt, D., Schuur, E. A. G., et al. (2020). Carbon release through abrupt permafrost thaw. *Nature Geoscience*, *13*(2), 138–143. https://doi.org/10.1038/s41561-019-0526-0

Watts, J. D., Natali, S. M., Minions, C., Risk, D., Arndt, K., Zona, D., et al. (2021). Soil respiration strongly offsets carbon uptake in Alaska and Northwest Canada. *Environmental Research Letters*, *16*, 084051. https://doi.org/10.1088/1748-9326/ac1222

Welker, J. M., Fahnestock, J. T., Henry, G. H. R., O'Dea, K. W., & Chimner, R. A. (2004). CO_2 exchange in three Canadian High Arctic ecosystems: Response to long-term experimental warming. *Global Change Biology*, *10*(12), 1981–1995. https://doi.org/10.1111/j.1365-2486.2004.00857.x

Welker, J. M., Fahnestock, J. T., & Jones, M. H. (2000). Annual CO_2 flux in dry and moist Arctic tundra: Field responses to increases in summer temperatures and winter snow depth. *Climatic Change*, *44*(1/2), 139–150. https://doi.org/10.1023/A:1005555012742

Winston, G. C., Sundquist, E. T., Stephens, B. B., & Trumbore, S. E. (1997). Winter CO_2 fluxes in a boreal forest. *Journal of Geophysical Research*, *102*(24), 28795–28804. https://doi.org/10.1029/97jd01115

Xu, X., Trumbore, S. E., Zheng, S., Southon, J. R., McDuffee, K. E., Luttgen, M., & Liu, J. C. (2007). Modifying a sealed tube zinc reduction method for preparation of AMS graphite targets: Reducing background and attaining high precision. *Nuclear Instruments and Methods in Physics Research Section B: Beam Interactions with Materials and Atoms*, *259*(1), 320–329. https://doi.org/10.1016/J.NIMB.2007.01.175

Zona, D., Gioli, B., Commane, R., Lindaas, J., Wofsy, S. C., Miller, C. E., et al. (2016). Cold season emissions dominate the Arctic tundra methane budget. *Proceedings of the National Academy of Sciences of the United States of America*, *113*(1), 40–45. https://doi.org/10.1073/pnas.1516017113